Molecular mechanisms of functional rescue mediated by P53 tumor suppressor mutations

Yu-Hong Tan [a], Y. Morris Chen [a], Xiang Ye [a], Qiang Lu [a], Vira Tretyachenko-Ladokhina [a], Wei Yang [c], Donald F. Senear [a], Ray Luo [a,b,*]

[a] Department of Molecular Biology and Biochemistry, University of California, Irvine, California, 92697
[b] Department of Biomedical Engineering, University of California, Irvine, California, 92697
[c] Department of Chemistry and Biochemistry, Florida State University, Tallahassee, Florida 32306

ARTICLE INFO

ABSTRACT

We have utilized both molecular dynamics simulations and solution biophysical measurements to investigate the rescue mechanism of mutation N235K, which plays a key role in the recently identified global suppressor motif of K235/Y239/R240 in the human p53 DNA-binding domain (DBD). Previous genetic analysis indicates that N235K alone rescues five out of six destabilized cancer mutants. However, the solution biophysical measurement shows that N235K generates only a slight increase to the stability of DBD, implying a rescue mechanism that is not a simple additive contribution to thermodynamic stability. Our molecular simulations show that the N235K substitution generates two non-native salt bridges with residues D186 and E198. We find that the nonnative salt bridges, D186-K235 and E198-K235, and a native salt bridge, E171-R249, are mutually exclusive, thus resulting in only a marginal increase in stability as compared to the wild type protein. When a destabilized V157F is paired with N235K, the native salt bridge E171-R249 is retained. In this context, the non-native salt bridges, D186-K235 and E198-K235, produce a net increase in stability as compared to V157F alone. A similar rescue mechanism may explain how N235K stabilize other highly unstable β-sandwich cancer mutants.

1. Introduction

Premalignant cells must overcome the physiological regulation of growth and programmed cell death (or apoptosis) in order to turn into aggressive and metastatic cancers. Therefore, inactivation of tumor suppressor proteins through the accumulation of gene mutations is a central transforming event. Prominent among these tumor suppressor genes is p53; mutant p53 genes have been found in about 50% of human tumors, [1] About 75% of these are missense mutations that express full-length, but functionally inactive, protein [1,2]. These mutations are concentrated within the DNA-binding core domain (DBD) of approximately 200 amino acids, a domain that is central to the function of p53 as a transcription factor [1].

The significance of p53 mutation to cancer biology and the predominance of missense mutations in DBD have motivated searches for potential second-site suppressor mutations. Three classes of missense cancer mutations have been identified based on their inactivation mechanisms, i.e.: 1) loss of DNA contacts, 2) local structural perturbation, and 3) unfolding of DBD [3]. Accordingly, rescue of cancer mutants in these three classes is expected to require three distinct classes of suppressor mutations, i.e.: 1) mutations that introduce additional DNA contacts, 2) mutations that correct local structural distortion, and 3) mutations that refold DBD [4]. For an example of the first of these three classes, rational design identified a suppressor mutation, T284R, that increases the DNA binding affinity of the particular contact mutants R273C and R273H by providing a new DNA contact [5]. Of course, the limitation of this approach and of rescue of DNA contact mutants in general is that each particular mutant is likely to require an individually tailored suppressor. The same limitation might be expected to extend to cancer mutants that disrupt local structure in the DNA-binding region.

In contrast, missense cancer mutations that unfold DBD but do not perturb local structures at the DNA binding interface extend the promise of a global rescue mechanism based on refolding of DBD. Since DBD denatures in a two-state process [6,7] a suppressor located anywhere in the structure that pushes the equilibrium in the direction of the folded state should contribute to the refolding of all destabilized cancer mutants. Prominent among these destabilized cancer mutants are the β-sandwich mutants for which thermodynamic destabilization is indicated to be the only inactivation mechanism [3].

Brachmann and co-workers demonstrated the feasibility of a genetic approach to select suppressors of p53 cancer mutations [8–10]. Initial screens identified several candidates [8]. Two of these,

* Corresponding author. Department of Molecular Biology and Biochemistry, University of California, Irvine, California, 92697. Tel.: +1 949 824 9528; fax: +1 949 824 8551.
  E-mail address: rluo@uci.edu (R. Luo).

Fig. 1. Local structure at K232 in the mouse p53 core domain, where white bonds are for hydrophobic residues, blue bonds are for basic residues, red bonds are for acidic residues, and green bonds are for polar residues.

N268D and N239Y, represent potential examples of more broadly targeted refolding suppressors. The DBD of N268D is more stable than that of the wild type and V143A, a strongly destabilized β-sandwich mutant, is rescued by N268D due to additive energetic effects on stability [4,11]. N239Y was also found to increase the stability of DBD, [4,11] a result explained by the recent crystallographic structure of a super stable quadruple mutant [12]. Subsequent PCR mutagenesis suggests a suppressor motif of K235/Y239/R240 [10]. Sixteen of the 30 tested cancer mutants were rescued by combinations of these suppressor mutations [10]. The group rescued includes six mutations located in the β-sandwich where the hydrophobic core is located, and three each in the L2/L3 loops and loop-sheet-helix. Of seven β-sandwich cancer mutants tested, only one, Y163C, is not rescued, which suggests a mechanism involving the refolding of the DNA-binding core domain by global stabilization [10].

As described above, the thermodynamic investigations of N239Y [4] indicate that it operates by this refolding mechanism. The proximity of R240 to the DNA binding interface indicates that it may function by introducing additional DNA contacts. However, the rescue mechanism of N235K, located in S8 of the β-sandwich, [13] is less clear. This is an important suppressor, particularly for destabilized β-sandwich mutants. N235K alone rescues five of six β-sandwich cancer mutants among the top 30 cancer mutants (Danziger et al., in preparation). Residue 232 in the mouse p53 DNA-binding core domain is lysine, i.e, the equivalent to K235 in human p53. In the crystallographic structure of the mouse DBD (2IOI) [14] shown in Fig. 1, K232 forms a salt bridge with E195, which corresponds to E198

in human p53. A potential salt bridge interaction with D183, which corresponds to D186 in human p53, is also noticeable. This is similar to the situation in N268D, which was shown to rescue certain human p53 cancer mutants due to formation of an additional salt bridge interaction. However in contrast to N268D which increases the stability of human p53 DBD by 1.2 kcal/mol, [4] N235K generates only a slight increase to the stability of the human p53 DBD, i.e. by 0.3 kcal/mol (Table 1). This implies a rescue mechanism that is not a simple additive contribution to thermodynamic stability. Due to the potential significance of N235K as a global cancer suppressor, the mechanism for its rescue of destabilized β-sandwich mutants, if not by simple contribution to global stability, poses a significant question.

In this study, we have used solution biophysical measurements and molecular simulations in explicit solvent to investigate the likely rescue mechanisms of N235K to restore unstable cancer mutants. Our focus on protein stability is based on the available crystal structures that show virtually no major difference between cancer mutants and the wild type DBD whether they are stable or not [15–17]. Our simulation design is also to bypass the difficulty in the stability analysis through direct simulation of protein folding/unfolding at room temperature. The first MD simulations of the p53 DNA-binding domain were reported as early as the beginning of this century, [18–26] though none of these previous MD studies focus on direct folding/unfolding simulations of the protein, which are clearly beyond the limit of current computational power. We have chosen two β-sandwich cancer mutants as test cases in our analysis of the rescue mechanisms of N235K. These are V157F, one of the most destabilizing cancer mutations, but which is refolded by N235K alone and Y163C, a similarly destabilized cancer mutant that is not refolded by N235K alone, though it can be in combination with other elements of the 235/239/240 suppressor motif.

2. Experimental Procedures

2.1. Molecular Dynamics Simulations

The atomic coordinates of the wild type p53 DBD were obtained from crystal structure 1TSR chain B [13]. The atomic coordinates of all mutants were obtained with the LEaP module of AMBER 9 [27] starting from the WT structure. All systems were solvated in a truncated octahedron box of TIP3P waters [28] with a buffer of 10 Å. Particle Mesh Ewald (PME) [29] was employed to treat long-range electrostatic interactions with the default setting in AMBER 9 [27]. A revised parm99 force field was used for intramolecular interactions [30,31]. The Zn-binding interface was modeled with a covalent approach with optimized bond and angle terms as documented in our previous study [21]. The SHAKE algorithm [32] was applied to constrain bonds involving hydrogen atoms. 1000-step steepest descent minimization was performed to relieve any structural clash in the solvated systems. This was followed by heating up for 10 ps in the NVT ensemble and equilibration of 1 ns in the NPT ensemble [33] at 283 K with PMEMD of AMBER 9 [27].

Table 1
High-temperature unfolding rate and relative thermodynamic stability for wild type and mutant p53 DBD's.

Protein		High temperature unfolding			Thermodynamic stability	
p53 allele	Functional description	t_1(ps)	Error(ps)	R^2	$\Delta\Delta G_{D:N}^{H_2O}$ (kcal/mol)	Reference
WT		6757	79	0.97	0.0	–
N235K	Rescue	6760	101	0.96	-0.3 ± 0.12	this work
V157F	Cancer	4062	52	0.98	3.9 ± 0.06	Bullock et al. (2000)
V157F/N235K	Cancer/rescue	6045	62	0.98	2.2 ± 0.13	this work
Y163C	Cancer	5364	62	0.98	3.5 ± 0.17	this work
Y163C/N235K	Cancer/rescue	5792	63	0.98	N.A.	N.A

Unfolding time constants (t_1), uncertainties (Error), and correlation coefficients (R^2) are from global fits of a single exponential decay model to the mean native contact fraction over 10 independent high-temperature molecular dynamics trajectories for each protein. Relative thermodynamic stability at 10 °C was determined by solvent denaturation as obtained in this work, or taken from the measurements by Bullock et al. [37]. N.A.: not available. Gibbs free energy changes are in the direction of folding. Thus, the differences in Gibbs free energy changes listed are related to the relative probability of the unfolded state according to $p_{unfolded} = e^{\Delta\Delta G/RT}$.

Langevin dynamics with γ of 1 ps^{-1} and a time step of 2 fs was used in the heating run. Molecular dynamics with τ_T of 2 ps and a time step of 2 fs was used in the equilibration run. All other parameters are set to be the default values in AMBER 9 [27].

All equilibration runs were continued with an accelerated molecular dynamics simulation with the recently developed essential energy space metadynamics algorithm to improve the convergence at room temperature [34]. To realize essential energy space random walk, a biasing potential $f_m(U_s)$, where essential energy U_s is defined as the sum of all the energy terms except for bond and angle ones, was obtained from a 1 ns essential energy space metadynamics simulations. The accelerated molecular dynamics trajectory was then obtained from 10 ns simulation, which was run with the addition of the biasing potential $f_m(U_s)$ [34].

2.2. High-temperature Unfolding Simulations

Our use of high-temperature unfolding simulations to probe protein stability is based on an earlier experimental study that demonstrated a high correlation between kinetic unfolding rates and thermodynamic stabilities of p53 DBD cancer mutants at body temperature [35]. It should be pointed out that two-state folding processes do not in general imply such a high correlation, the so-called "kinetic instability" effect [35]. This is because kinetic unfolding rates may change not because of the changes in relative stability of folded v.s. unfolded states but because of the changes in stability of transition state. Thus the "kinetic instability" effect indicates that the kinetic folding rates of p53 DBD cancer mutants must be very similar (for two-state protein folding processes, $K = k_f / k_u$, where K is the folding equilibrium constant, k_f and k_u are folding and unfolding rates, respectively), i.e. the folding activation free energy is mostly insensitive to cancer mutations, as confirmed directly in a recent study [36]. These observations show that we can focus on unfolding in the study of protein DBD stabilities, which dramatically simplifies our simulation difficulty of such a large protein to probe the mechanisms in the loss or gain of stability upon mutations.

Additionally, the p53 core domains fold via multiple pathways, ranging from a few seconds to more than a few hours under strongly native conditions [36]. What further complicates the interpretation is the observation that folding intermediates are susceptible to dead-end aggregation, thereby providing a kinetic trap [36]. However the aggregated states disappear at high urea concentration where the thermodynamic analysis was conducted [36] so that the urea denaturation data can still be correctly interpreted as two-state folding. This is consistent with the long history of successful two-state analysis by the Fersht group [4,6,37,38]. Nevertheless, this interpretation does not apply to the slow folding pathways that have intermediates. Such an interpretation of the urea denaturation data further simplifies our computational analysis of the p53 core domain unfolding by focusing on very fast pathways in our simulations, i.e. *we shall bypass the slow pathways by running short unfolding trajectories only*. To study the two-state fast unfolding kinetics of each solvated protein, 10 independent unfolding trajectories of 10 ns each at 483 K were generated after heating the system for 10 ps in Langevin dynamics with PMEMD of AMBER 9 [27]. The snapshots were saved every 10 ps. The use of 10 independent trajectories was to increase the statistical certainty in the use of otherwise very short trajectories. Of course, the proteins can only unfold fractionally in such a short time (up to 50% only) even if the very high simulation temperature was used. We found that even 20 ns high-temperature simulation results in multi-phase unfolding kinetics, i.e. poor fitting with respect to the single-exponential decay.

A total of ~1,000 ns trajectories were collected for all solvated proteins (WT, V157F, N235K, V157F/N235K, Y163C, Y163C/N235K, one control for V157F/N235K, one control for N235K, and one control for WT) at both 283 K and 483 K, respectively. Native contact assignment was handled with in-house software. Two residues ($i, i + 3$ and beyond)

are in contact when their Cα atoms are closer than 6 Å. All distance calculations were conducted with PTRAJ in AMBER 9 [27]. The time-dependence of unfolding kinetics was fitted using Origin. The kinetic traces were fitted well by a single exponential function as: $Q = Q_0 + A_1 \cdot \exp(-t/t_1)$. A salt bridge is defined when the distance between any two charged heavy atoms (for example O$^-$, N$^+$) is less than or equal to 3.2 Å.

2.3. Solvent Denaturation

Experimental equilibrium unfolding of p53 DBD was monitored by unfolding-induced changes in its intrinsic fluorescence as described by Fersht and colleagues [6]. Individual p53 samples in 50 mM sodium phosphate buffer, pH 7.2, containing 5 mM DTT plus urea at concentrations ranging from 0 to 5.5 M were incubated overnight at 10 °C. Fluorescence emission spectra (average of 20 scans) were recorded from 300 to 370 nm in an SLM-8100 spectra flourimeter in 2×10 mm cuvettes in a Peltier-controlled cell holder at 10 °C. Excitation was at 280 nm and the bandpass was 8 nm on both excitation and emission. Folded p53 DBD generates a characteristic emission spectrum with a peak at 305 nm and a long tail extending to the red [6] reflecting strong contributions from some or all of its 6 tyrosine residues and weaker contributions from its 3 tryptophan residues. Unfolded monomeric p53 DBD is characterized by a decrease in 305 nm emission and appearance of a peak at around 350 nm, consistent with increased tryptophan emission. An isofluorescence point at about 320 nm is indicative of a two-state unfolding transition. Baseline-subtracted spectra were normalized using the isofluorescence for all variants except V157F. Unfolded and aggregated p53 is characterized by broad emission with a maximum near 330 nm [6]. A small amount of this material that was present in V157F samples precluded normalization. The difference in intensity, $I_{356} - I_{305}$, was analyzed according to the linear extrapolation model [39]. This assumes a two-state unfolding model and linear dependence of unfolding free energy on denaturant concentration. The model, as formulated by Santora and Bolen [40] is given by

$$I_{obs} = (I_N + m_N[D]) + (I_U + m_U[D])\frac{\exp(-(\Delta G_{N-U} + m_D[D])/RT)}{1 + \exp(-(\Delta G_{N-U} + m_D[D])/RT)},$$

where I_N and I_U represent the intercepts, and m_N and m_U the slopes of the pre- (native protein) and post- (unfolded protein) baselines, while ΔG_{N-U} is the unfolding free energy change in the absence of denaturant, and m_D the slope of its linear dependence on denaturant concentration, [D]. Data were fitted using Origin. Given a linear dependence of ΔG_{D-N} on urea concentration, the folding stability in the absence of denaturant is approximated well by $\Delta G_{D-N}^{H_2O} = <m_{urea}> \cdot [urea]_{0.5}$, where $<m_{urea}>$ is the average slope.

3. Results and Discussion

3.1. High-temperature unfolding rates and correlation to stabilities

Temperature-induced unfolding of the wild type p53 DBD and of several mutants (N235K, V157F, V157F/N235K, Y163C, Y163C/N235K) was studied using high-temperature molecular dynamics simulations in explicit solvent. The degree of unfolding was assessed by calculating the average fraction of native contacts (Q) remaining at a given time point after the temperature jump. The values plotted for each protein in Fig. 2 represent the average of 10 independent trajectories. A single exponential decay function was found to fit the early unfolding transition for each of the proteins (Fig. 2). Parameters obtained from these fits are listed in Table 1.

Table 1 also presents the relative thermodynamic stability for each mutant at 283 K as compared to the wild type DBD. These were obtained from solvent (urea) denaturation studies, under which conditions, both wild type and mutant p53 DBD's denature reversibly in a two-state transition. The differences in Gibbs free energy changes
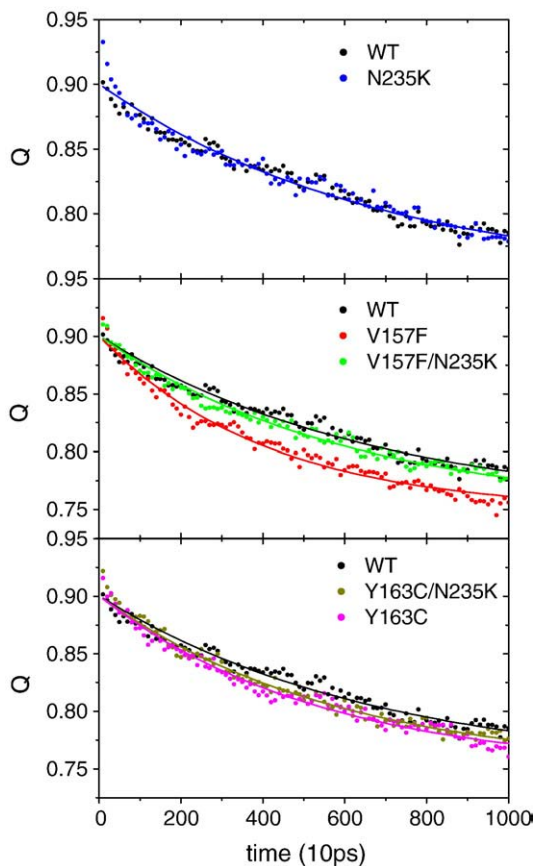
Fig. 2. Native contact fraction in unfolding of WT, N235K, V157F, V157F/N235K, Y163C, and Y163C/N235K. The simulated native contact fractions are averaged over 10 independent trajectories for each protein.

listed reflect the difference in the relative probability of the unfolded state in the absence of urea. Positive values indicate a higher proportion of unfolded molecules, or lower stability. Comparison of unfolding rates (Fig. 2 & Table 1) to thermodynamic stability (Table 1) shows a clear correlation between protein stability and time-dependent preservation of native contacts at high temperature. More specifically, a longer unfolding half time (t_1) is observed for protein of higher stability. This observation is consistent with an earlier experimental study on the kinetic unfolding rates and thermodynamic stabilities of p53 DBD cancer mutants at body temperature [35]. Based on this finding, we have compared the preservation of native contacts and the unfolding half times to assess the effects of suppressor mutations on the stabilities of wild type p53 and p53 cancer mutations.

3.2. Effect of N235K on stability of wild type DBD

As described above, a striking difference between suppressor mutant N235K and other stabilizing suppressor mutations, such as N239Y and N268D, is its marginal stabilizing effect on the WT protein (Fig. 2 and Table 1). Structural analysis of the mouse WT structure, reveals two potential salt bridge interactions in that structure, D183-K232 and E195-K232, whose human homologs, D186-K235 and E198-K235, are likely to form when N235 is mutated to lysine (Fig. 1). Fig. 3 shows the occupancy of these two salt bridges in the unfolding simulation of N235K. The occupancy of both salt bridges remains high during the early phase of unfolding. In contrast to this behavior exhibited by the new salt bridges generated by the K235 substitution, systematic evaluation of all intramolecular salt bridges reveals that another important salt-bridge in the wild type DBD structure, E171-R249, is disrupted in the N235K
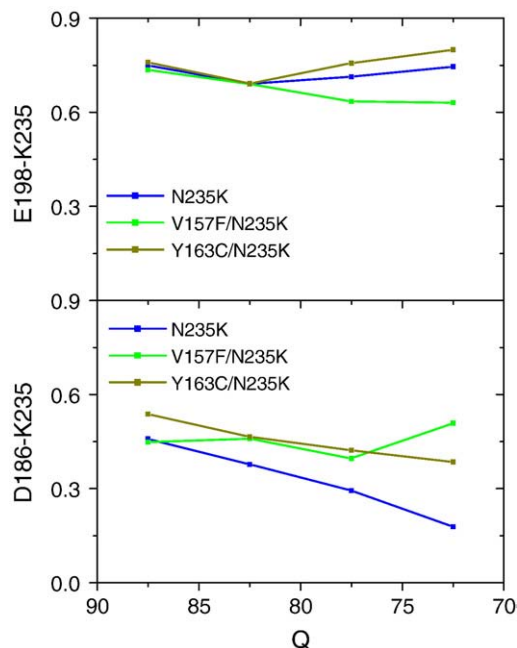

Fig. 3. Occupancy of salt bridge E198-K235 (upper) and D186-K235 (lower) in N235K, V157F/N235K and Y163C/N235K.

structure. The occupancy of this salt bridge is reduced compared to wild type DBD and decreases more rapidly during the unfolding transition (Fig. 4).
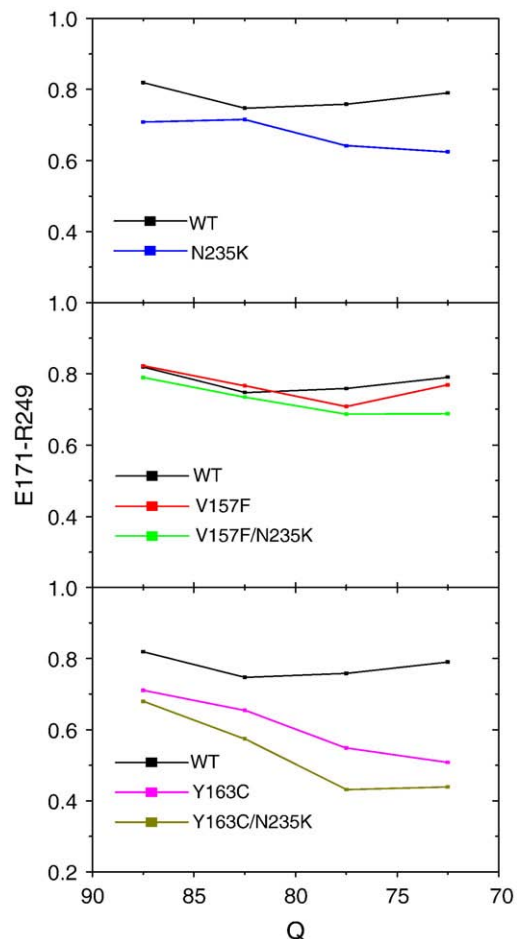

Fig. 4. Occupancy of salt bridge E171-R249 in WT, N235K, V157F, V157F/N235K, Y163C, and Y163C/N235K.

We note that loss of a salt bridge does not always result in a significant decrease in protein stability. To assess the contribution of the E171-R249 salt bridge on the stability of wild type p53 DBD, we performed unfolding of wild type p53 DBD in which both E171 and R249 were neutralized (i.e. GLU replaced by GLH and ARG replaced by ARN in the AMBER force field). Fig. 5 compares the unfolding of neutralized and native wild type proteins. Kinetic parameters obtained by fitting the trajectories as described earlier are listed in Table 2. Neutralization of both partners of this salt bridge results in both a decrease in the number of native contacts (Fig. 5) and an increase in the rate of unfolding (Table 2), indicating a less stable protein. Thus we conclude that the E171-R249 contact contributes significantly to p53 DBD stability. Apparently this analysis does not exclude additional structural effects of the N235K mutation, [41] which is not the focus of our study.

Nevertheless, the conclusion that the loss of the E171-R249 salt bridge contributes significantly to the loss of stability is also supported by experimental observations reported previously. R249S is a naturally occurring cancer mutant that disrupts this salt bridge and is reported to destabilize the p53 DBD by 1.9 kcal/mol [4,6,37]. R249 is located on loop L3 where it is largely solvent-exposed. Consequently, substitution of serine for argentine at this location would be expected to have little effect on the hydrophobic core of the DBD. Thus the stability loss upon mutation R249S should primarily be due to the loss of salt bridge E171-R249.

To confirm that the non-native salt bridges introduced by K235 are responsible for the disruption of salt bridge E171-R249, we performed unfolding simulations in which K235 was neutralized (i.e. LYS replaced by LYN in the AMBER force field). This results in decreased stability relative to N235K (Fig. 6 and Table 2). While the neutral side chain still interacts with E198 and D186, the strength of these dipole-charge interactions decreases as a function of distance much more rapidly than the salt bridges made by charged side chains. Consequently, the interactions between LYN 235 and the two carboxylates of E198 and D186 are weaker than the E198-K235 and D186-K235 interactions when the protein is in the process of unfolding. At the same time, the simulations indicate higher occupancy of the E171-R249 interaction for N235 LYN as compared to N235K in the process of unfolding (Fig. 6). This establishes a direct correlation between E171-R249 and interactions between residue 235 and the two carboxylates of E198 and D186 as summarized below. In the wild type protein, N235 (a much shorter side chain) has little interaction with either E198 or D186 and the E171-R249 salt bridge is nearly 80% occupied (Fig. 6). LYN 235 has weak interactions with the two carboxylates and E171-R249 is slightly destabilized (Fig. 6). K235 has stronger interactions with the two carboxylates and E171-R249 is significantly
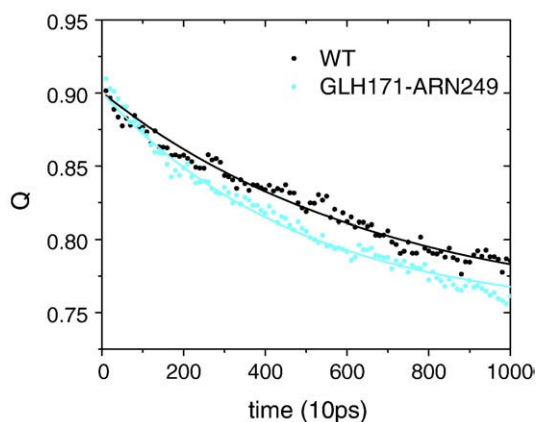
destabilized (Fig. 6). Thus, the competition between D186-K235/E198-K235 on the one hand and E171-R249 on the other explains why N235K generates only a marginal increase in stability compared to wild type DBD.

While mutual disruption of the D186-K235/E198-K235 and E171-R249 salt bridges is an observation in the unfolding simulations, we can only speculate about the underlying coupling mechanism. We note that these competing interactions are located at opposite sides of an intact and tightly packed hydrophobic core (Fig. 7). Presumably it is the rigidity of this structure that prevents optimal geometry for making both sets of interactions simultaneously.

3.3. Refolding of V157F by N235K

Although N235K affects the stability of the wild type p53 DBD to only a marginal extent it functions quite broadly to rescue β-sandwich cancer mutants *in vivo*. Global destabilization of the folded DBD structure is believed to be the only cause of inactivation of β-sandwich cancer mutants. Given its failure to stabilize the wild type DBD, by what mechanism does N235K rescue β-sandwich cancer mutants? Either N235K is selectively able to refold β-sandwich cancer mutants, or rescue is by an entirely different mechanism.

Table 2
High-temperature unfolding time constants t_1, their uncertainties (Error), and R^2 for the three sets of the high-temperature control simulations with neutralized salt bridges.

Proteins	t_1(ps)	Error(ps)	R^2
WT	6757	79	0.97
WT(GLH171-ARN249)	4839	52	0.98
N235K	6760	101	0.96
N235 LYN	6273	86	0.95
V157F/N235K	6045	62	0.98
V157F/N235 LYN	4923	58	0.98

For clarity, related simulations from Table 1 are also shown here.

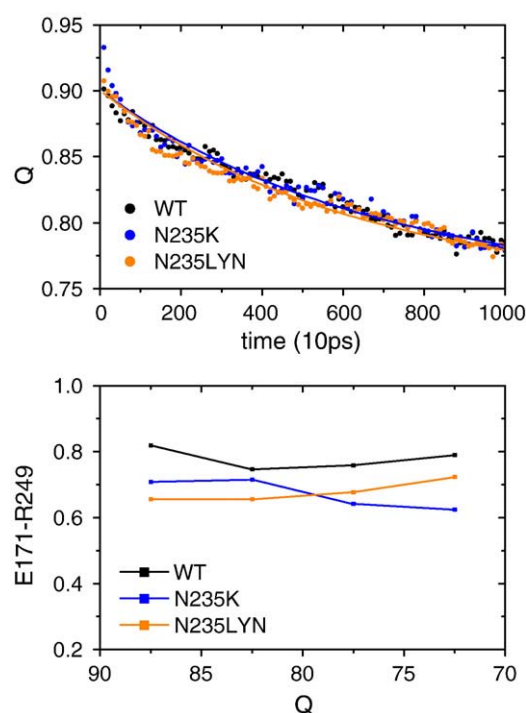Fig. 5. Native contact fraction in unfolding of WT, and WT with neutralized E171-R249 (GLH171-ARN249).

Fig. 6. Upper: Native contact fraction in unfolding of WT, N235K, and N235 LYN; Lower: occupancy of salt bridge E171-R249 in WT, N235K, and N235 LYN.
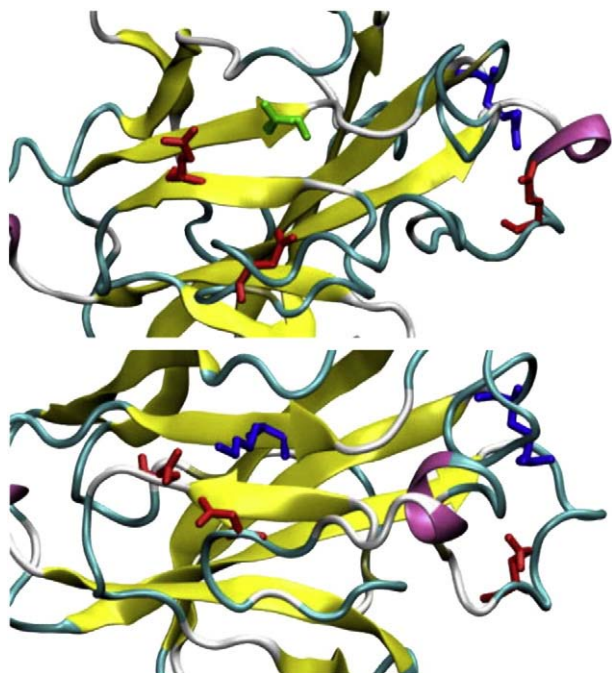
Fig. 9. Native contact fraction in unfolding of WT, V157F/N235K and V157F/N235 LYN.

To explore the difference in effects due to K235 on wild type versus V157F DBD's, we evaluated the non-native salt bridges, D186-K235 and E198-K235, in unfolding simulations of the V157F/N235K cancer/suppressor pair mutant. We also evaluated the E171-R249 salt bridge in both cancer alone (V157F) and cancer/suppressor pair mutants. The non-native salt bridges D186-K235 and E198-K235 remain highly occupied in V157F/N235K throughout the unfolding simulation (Fig. 3). In addition, the occupancies for the native salt bridge, E171-R249, also remain high throughout the unfolding simulation (Fig. 4), distinctly higher than for N235K alone and similar to WT DBD. Thus, the competition between salt bridges D186-K235/E198-K235 and E171-R249 as observed in the suppressor mutant N235K does not occur in the cancer/suppressor mutant V157F/N235K. Salt bridge E171-R249 has largely survived the structural perturbation due to salt bridges D186-K235 and E198-K235. The underlying reason for the strikingly different responses to the N235K mutation in WT versus V157F may lie in effect of V157F on the hydrophobic packing in the center of the β-sandwich core. We hypothesize that the packing perturbation due to substitution by the bulkier phenyl side chain of the mutant disrupts the obligatory structural coupling between salt bridge interactions that lie at opposite side of the core, thus allowing simultaneous formation of all three salt bridges.

To test the hypothesis that the formation of two salt bridges D186-K235 and E198-K235 causes a stability gain in V157F/N235K, we performed unfolding simulations in which LYS 235 was neutralized to LYN. Fig. 9 compares the unfolding trajectories for WT, V157F/N235K and V157F/N235 LYN. Kinetic parameters for all three are listed in Table 2. As is clear from these comparisons, the non-native salt bridges made by K235 contribute significantly to the stability of the V157F/N235K cancer/suppressor mutant.

Fig. 7. Salt bridges (D186-K235/E198-K235 and E171-R249) at the two opposite sides of the hydrophobic core in WT (upper) and in N235K (lower). See Fig. 1 for color coding scheme.

β-sandwich cancer mutant V157F was chosen as a model to address this question. Fig. 8 shows the local structure near V157F. Substitution of the bulkier phenyl group necessarily wedges apart the two sheets that comprise the β-sandwich, thus destabilizing the hydrophobic core. In unfolding simulations, as shown in Fig. 2, native contacts are lost more rapidly for V157F than for WT. Indeed, V157F unfolds the fastest among all proteins analyzed, consistent with its relative stability, which is about 4 kcal/mol below wild type DBD, making V157F the least stable of all proteins studied (Table 1). Both behaviors are partially reversed in the double mutant, V157F/N235K, in which cancer and suppressor mutations are paired (Fig. 2 and Table 1). Both the rate of unfolding and the thermodynamic stability are restored by about half of the deleterious effect due to the cancer mutant alone. Though still destabilized compared to wild type DBD, the amount is insufficient to account for loss of function in vivo [37]. Thus we conclude that N235K can uniquely refold β-sandwich cancer mutants to functional levels.
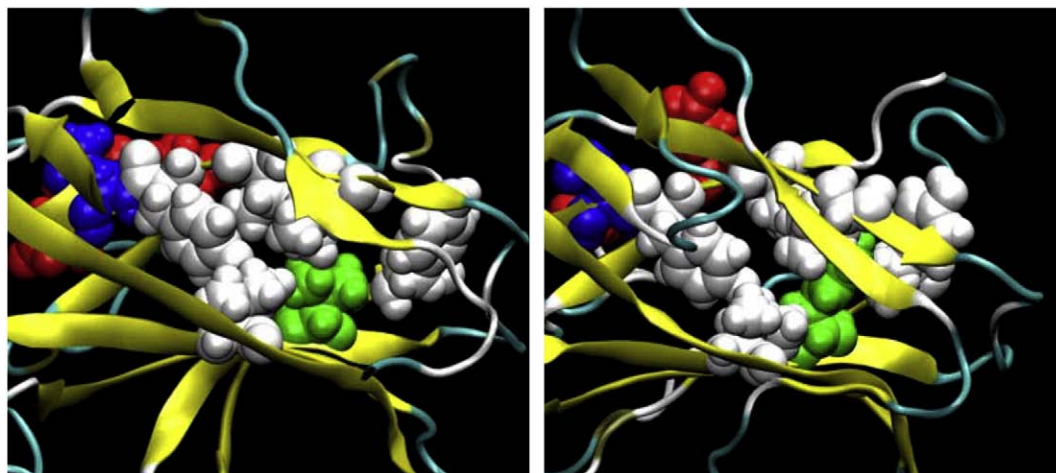

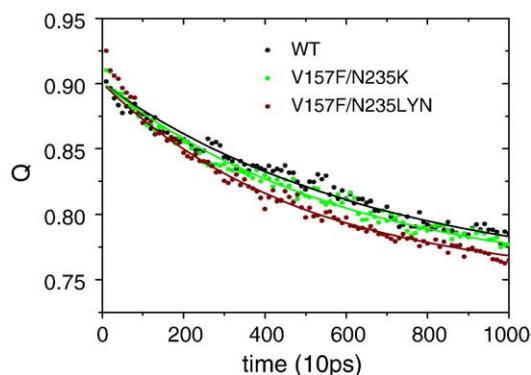Fig. 8. Mutation site V157F in WT (left) and in V157F (right). See Fig. 1 for color coding scheme.
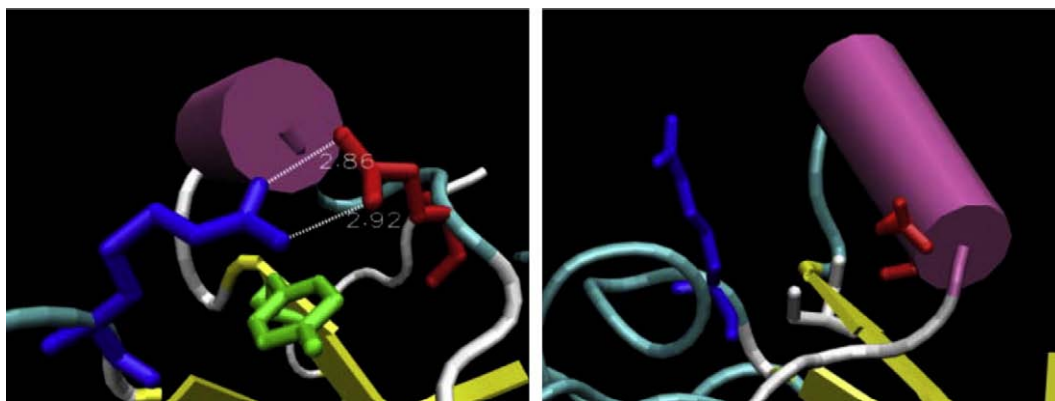
Fig. 10. Mutation site Y163C in WT (left) and in Y163C (right). See Fig. 1 for color coding scheme.

3.4. Resistance of Y163C to Refolding by N235K

Cancer mutant Y163C presents an interesting negative control for our analysis of the refolding mechanism generated by N235K. Following the same strategy as employed to investigate refolding of V157F, we first analyzed why Y163C is destabilizing. Fig. 10 compares the local structures in the vicinity of the wild type side chain, Y163 (left) and a model of the mutant, Y163C (right). The salt bridge, E171-R249, is packed directly above Y163 exposing only one side to solvent. Substitution of the smaller hydrophilic cystine side-chain for the hydrophobic phenol group in Y163C exposes both faces of the salt bridge to solvent and invites water to compete for the favorable electrostatic interactions from both sides. This is expected to significantly weaken the salt bridge. Indeed, as shown in Fig. 4 the occupancy of salt bridge E171-R249 is significantly lower in Y163C than in WT. As discussed above, E171-R249 is very important to the stability of p53 core domain, supporting the argument that Y163C destabilizes p53 in this manner.

Thus in contrast to V157F, in which the E171-R249 salt bridge is retained, this interaction is always absent in Y163C in a manner that is not subject to refolding by a remote suppressor mutation. As proposed above, the potential gain in stability due to formation of the additional non-native salt-bridges D186-K235 and E198-K235 in N235K is counterbalanced by the loss of WT salt bridge E171-R249. We propose that it is precisely due to this competition that the suppressor mutant N235K is only marginally more stable than the wild type DBD. Cancer mutation Y163C further weakens salt bridge E171-R249. Indeed, the salt bridge E171-R249 occupancy is the lowest in Y163C/N235K among all the proteins analyzed (Fig. 4). V157F is destabilized due to disruption of the packing in the hydrophobic core and despite its retention of salt bridge E171-R249. The packing disruption also uncouples this salt bridge from the additional non-native salt bridges that involve N235K, thus allowing the additional salt bridges to compensate in part for the disruption of the core packing. We presume a similar mechanism for most β-sandwich cancer mutants. Y163C is unique in its loss of salt bridge E171-R249, and due to solvent exposure, a mechanism that is not reversible by a remote suppressor mutation. Thus, it is impossible for N235K to refold Y163C.

3.5. Limitations of the Approach

Our primary motivation in this study is to probe the mechanisms of N235K to restore the stability of unstable cancer mutants. Our focus on protein stability and protein unfolding is based on the experimental findings: (1) there is virtually no difference among available crystal structures of destabilized cancer mutants and the wild type protein, and (2) there is a high correlation between unfolding rates and stabilities among destabilized cancer mutants and the wild type protein. Specifically, high temperature unfolding simulation strategy is used to study the difference of the denatured proteins. Apparently our use of high temperature simulations can only lead to qualitative conclusions on the rescue mechanisms of N235K at the experimental condition.

Further it is not our intentions to study the complex unfolding pathways of DBD. This subject is clearly very interesting and will be addressed in our future studies. In addition, the major findings in this study are based primarily on computational results. The results suggest additional experiments that could be used to test the conclusions. For example, one could use double (or triple) mutants to test the involvement of the E171-R249 salt bridge that we propose plays a critical role in how the N235K mutant refolds the V157F cancer mutant without significantly affecting stability of the wild-type. Although beyond the scope of the present study, this is included in our future studies.

References

[1] M. Olivier, R. Eeles, M. Hollstein, M. Khan, C. Harris, P. Hainaut, The iarc tp53 database: New online mutation analysis and recommendations to users, Hum. Mutat. 19 (2002) 607–614.

[2] A.C.R. Martin, A.M. Facchiano, A.L. Cuff, T. Hernandez-Boussard, M. Olivier, P. Hainaut, J.M. Thornton, Integrating mutation data and structural analysis of the tp53 tumor, suppressor protein, Hum. Mutat. 19 (2002) 149–164.

[3] A.N. Bullock, A.R. Fersht, Rescuing the function of mutant p53, Nat. Rev. Cancer 1 (2001) 68–76.

[4] P. Nikolova, K. Wong, B. Dedecker, J. Henckel, A. Fersht, Mechanism of rescue of common p53 cancer mutations by second-site suppressor mutations, EMBO J. 19 (2000) 370–378.

[5] A.M. Wieczorek, J.L.F. Waterman, M.J.F. Waterman, T.D. Halazonetis, Structure-based rescue of common tumor-derived p53 mutants, Nat. Med. 2 (1996) 1143–1146.

[6] A.N. Bullock, J. Henckel, B.S. Dedecker, C.M. Johnson, P.V. Nikolova, M.R. Proctor, D.P. Lane, A.R. Fersht, Thermodynamic stability of wild-type and mutant p53 core domain, Proc. Natl. Acad. Sci. U. S. A. 94 (1997) 14338–14342.

[7] J.S. Butler, S.N. Loh, Structure, function, and aggregation of the zinc-free form of the p53 DNA binding domain, Biochemistry-Us 42 (2003) 2396–2403.

[8] R.K. Brachmann, K.X. Yu, Y. Eby, N.P. Pavletich, J.D. Boeke, Genetic selection of intragenic suppressor mutations that reverse the effect of common p53 cancer mutations, EMBO J. 17 (1998) 1847–1859.

[9] T. Kobayashi, T. Wang, H. Qian, R.K. Brachmann, Genetic strategies in s. Cerevisiae to study human tumor suppressor genes, Methods Mol. Biol. 223 (2003) 73–86.

[10] T.E. Baroni, T. Wang, H. Qian, L.R. Dearth, L.N. Truong, J. Zeng, A.E. Denes, S.W. Chen, R.K. Brachmann, A global suppressor motif for p53 cancer mutants, Proc. Natl. Acad. Sci. U. S. A. 101 (2004) 4930–4935.

[11] K.B. Wong, B.S. Dedecker, S.M.V. Freund, M.R. Proctor, M. Bycroft, A.R. Fersht, Hot-spot mutants of p53 core domain evince characteristic local structural changes, Proc. Natl. Acad. Sci. U. S. A. 96 (1999) 8438–8442.

[12] A.C. Joerger, M.D. Allen, A.R. Fersht, Crystal structure of a superstable mutant of human p53 core domain - insights into the mechanism of rescuing oncogenic mutations, J. Biol. Chem. 279 (2004) 1291–1296.

[13] Y. Cho, S. Gorina, P.D. Jeffrey, N.P. Pavletich, Crystal structure of a p53 tumor suppressor-DNA complex: Understanding tumorigenic mutations, Science 265 (1994) 346–355.

[14] W.C. Ho, C. Luo, K.H. Zhao, X.M. Chai, M.X. Fitzgerald, R. Marmorstein, High-resolution structure of the p53 core domain: Implications for binding small-molecule stabilizing compounds, Acta Crystallogr. D 62 (2006) 1484–1493.

[15] A.C. Joerger, H.C. Ang, A.R. Fersht, Structural basis for understanding oncogenic p53 mutations and designing rescue drugs, Proc. Natl. Acad. Sci. U. S. A. 103 (2006) 15056–15061.

[16] A.C. Joerger, H.C. Ang, D.B. Veprintsev, C.M. Blair, A.R. Fersht, Structures of p53 cancer mutants and mechanism of rescue by second-site suppressor mutations, J. Biol. Chem. 280 (2005) 16030–16037.

[17] T. C., T.Y. H., S. G., Z. Z., B. Y., L. R., J. X., Impact of low-frequency hotspot mutation r282q on the structure of p53 DNA-binding domain as revealed by crystallography at 1.54 a resolution, Acta Crystallogr., D Biol. Crystallogr. 64 (2008) 471–477.

[18] S.Y. Noskov, J.D. Wright, C. Lim, Long-range effects of mutating r248 to q/w in the p53 core domain, J. Phys. Chem. B 106 (2002) 13047–13057.

[19] J.D. Wright, S.Y. Noskov, C. Lim, Factors governing loss and rescue of DNA binding upon single and double mutations in the p53 core domain, Nucleic Acids Res. 30 (2002) 1563–1574.

[20] Y.P. Pan, B.Y. Ma, R.B. Venkataraghavan, A.J. Levine, R. Nussinov, In the quest for stable rescuing mutants of p53: Computational mutagenesis of flexible loop l1, Biochemistry-Us 44 (2005) 1423–1432.

[21] Q. Lu, Y.H. Tan, R. Luo, Molecular dynamics simulations of p53 DNA-binding domain, J. Phys. Chem. B 111 (2007) 11538–11545.

[22] Y.P. Pan, R. Nussinov, Structural basis for p53 binding-induced DNA bending, J. Biol. Chem. 282 (2007) 691–699.

[23] B. Ma, A.J. Levine, Probing potential binding modes of the p53 tetramer to DNA based on the symmetries encoded in p53 response elements, Nucleic Acids Res. 35 (2007) 7733–7747.

[24] Y.P. Pan, R. Nussinov, P53-induced DNA bending: The interplay between p53-ona and p53–p53 interactions, J. Phys. Chem. B 112 (2008) 6716–6724.

[25] A. Madhumalar, D.J. Smith, C. Verma, Stability of the core domain of p53: Insights from computer simulations, BMC Bioinformatics 9 (2008) Article No.: S17.

[26] A. Madhumalar, L.H. Jun, D.P. Lane, C.S. Verma, Dimerization of the core domain of the p53 family a computational study, Cell Cycle 8 (2009) 137–148.

[27] D. Case, T. Darden, T. Cheatham Iii, C. Simmerling, J. Wang, R. Duke, R. Luo, K. Merz, B. Wang, D. Pearlman, M. Crowley, S. Brozell, V. Tsui, H. Gohlke, J. Mongan, V. Hornak, G. Cui, P. Beroza, C. Schafmeister, J. Caldwell, W. Ross, P. Kollman, Amber, AMBER 8, University of California, San Francisco, 8 ed., Regents of University of California, San Francisco, 2004.

[28] W.L. Jorgensen, J. Chandrasekhar, J.D. Madura, R.W. Impey, M.L. Klein, Comparison of simple potential functions for simulating liquid water, J. Chem. Phys. 79 (1983) 926–935.

[29] T. Darden, D. York, L. Pedersen, Particle mesh ewald - an n.Log(n) method for ewald sums in large systems, J. Chem. Phys. 98 (1993) 10089–10092.

[30] J.M. Wang, P. Cieplak, P.A. Kollman, How well does a restrained electrostatic potential (resp) model perform in calculating conformational energies of organic and biological molecules? J. Comput. Chem. 21 (2000) 1049–1074.

[31] T.Z. Lwin, R. Luo, Force field influences in beta-hairpin folding simulations, Protein Sci. 15 (2006) 2642–2655.

[32] J.P. Ryckaert, G. Ciccotti, H.J.C. Berendsen, Numerical-integration of cartesian equations of motion of a system with constraints - molecular-dynamics of n-alkanes, J. Comput. Phys. 23 (1977) 327–341.

[33] H.J.C. Berendsen, J.P.M. Postma, W.F. Vangunsteren, A. Dinola, J.R. Haak, Molecular-dynamics with coupling to an external bath, J. Chem. Phys. 81 (1984) 3684–3690.

[34] H. Li, D. Min, Y. Liu, W. Yang, Essential energy space random walk via energy space metadynamics method to accelerate molecular dynamics simulations, J. Chem. Phys. 127 (2007) 094101.

[35] A. Friedler, D.B. Veprintsev, L.O. Hansson, A.R. Fersht, Kinetic instability of p53 core domain mutants - implications for rescue by small molecules, J. Biol. Chem. 278 (2003) 24108–24112.

[36] J.S. Butler, S.N. Loh, Kinetic partitioning during folding of the p53 DNA binding domain, J. Mol. Biol. 350 (2005) 906–918.

[37] A. Bullock, J. Henckel, A. Fersht, Quantitative analysis of residual folding and DNA binding in mutant p53 core domain: Definition of mutant states for rescue in cancer therapy, Oncogene 19 (2000) 1245–1256.

[38] A. Friedler, L.O. Hansson, D.B. Veprintsev, S.M.V. Freund, T.M. Rippin, P.V. Nikolova, M.R. Proctor, S. Rudiger, A.R. Fersht, A peptide that binds and stabilizes p53 core domain: Chaperone strategy for rescue of oncogenic mutants, Proc. Natl. Acad. Sci. U. S. A. 99 (2002) 937–942.

[39] C.N. Pace, Determination and analysis of urea and guanidine hydrochloride denaturation curves, Methods Enzymol. 131 (1986) 266–280.

[40] M.M. Santoro, D.W. Bolen, Unfolding free-energy changes determined by the linear extrapolation method .1. Unfolding of phenylmethanesulfonyl alpha-chymotrypsin using different denaturants, Biochemistry-Us 27 (1988) 8063–8068.

[41] Y. Wang, A. Rosengarth, H. Luecke, Structure of the human p53 core domain in the absence of DNA, Acta Crystallogr. D 63 (2007) 276–281.